analytical chemistry

Article

pubs.acs.org/ac

Cytoplasmic RNA in Undifferentiated Neural Stem Cells: A Potential Label-Free Raman Spectral Marker for Assessing the Undifferentiated Status

Adrian Ghita,[†] Flavius C. Pascut,[†] Melissa Mather,[‡] Virginie Sottile,*[,§] and Ioan Notingher*[,†]

[†]School of Physics and Astronomy, [‡]School of Electrical and Electronic Engineering, and [§]School of Clinical Sciences, University of Nottingham, University Park, Nottingham NG7 2RD, U.K.

Supporting Information

ABSTRACT: Raman microspectroscopy (rms) was used to identify, image, and quantify potential molecular markers for label-free monitoring the differentiation status of live neural stem cells (NSCs) in vitro. Label-free noninvasive techniques for characterization of NCSs in vitro are needed as they can be developed for real-time monitoring of live cells. Principal component analysis (PCA) and linear discriminant analysis (LDA) models based on Raman spectra of undifferentiated NSCs and NSC-derived glial cells enabled discrimination of NSCs with 89.4% sensitivity and 96.4% specificity. The differences between Raman spectra of NSCs and glial cells indicated that the discrimination of the NSCs was based on higher concentration of nucleic acids in NSCs. Spectral images corresponding to Raman bands assigned to nucleic acids for individual NSCs and glial cells were compared with fluorescence staining of cell nuclei and cytoplasm to show that the origin of the spectral differences were related to cytoplasmic RNA. On the basis of calibration models, the concentration of the RNA was quantified and mapped in individual cells at a resolution of ~700 nm. The spectral maps revealed cytoplasmic regions with concentrations of RNA as high as 4 mg/mL for NSCs while the RNA concentration in the cytoplasm of the glial cells was below the detection limit of our instrument (~1 mg/mL). In the light of recent reports describing the importance of the RNAs in stem cell populations, we propose that the observed high concentration of cytoplasmic RNAs in NSCs compared to glial cells is related to the repressed translation of mRNAs, higher concentrations of large noncoding RNAs in the cytoplasm as well as their lower cytoplasm volume. While this study demonstrates the potential of using rms for label-free assessment of live NSCs in vitro, further studies are required to establish the exact origin of the increased contribution of the cytoplasmic RNA.

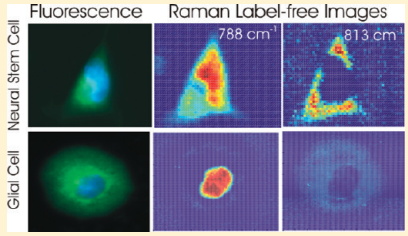

Neural stem cell-based therapies are emerging approaches opening radically new strategies for the treatment of neurological diseases.[1] Currently, neurological diseases are one of the leading causes of adult disability, and it is estimated that by 2040 neurological diseases will surpass cancer as the second most common cause of death among elderly people.[2] In light of our aging population, the development of effective therapeutic strategies for neurological disorders is of great importance. Although the potential clinical impact of stem cell therapy for neurological diseases has already been shown,[3] there are still a number of challenges to overcome before it can be considered suitable for widespread, long-term use. One such challenge is the identification of appropriate cell sources and the maintenance of a stable cell phenotype during the necessary phase of in vitro expansion. Current approaches for the characterization of neural stem cells (NSCs) in vitro are experimentally intensive, often employ destructive assays[4] rendering time-course experiments impossible, or are based on crude estimates, such as morphological features,[5] which are insufficient to provide insight into molecular cellular processes. In order to address fundamental questions necessary for process discovery and development of robust cell cultures for cellular therapy, new methodologies capable of quantifying key biomarkers in a noninvasive manner are urgently needed.[6]

Conventional cell biology assays (e.g., polymerase chain reaction, Western blotting, etc) are invasive and are not suitable for characterizing heterogeneous cell populations since they require a large number of cells and results represent averages over entire cell populations.[4] Fluorescence imaging can provide high-spatial resolution information for cells in vivo and in vitro, but often relies on lineage-specific surface markers that are expressed on the cell membrane.[7] However, there are numerous cases, including NSCs, where the major lineage specific markers are intracellular targets and detection requires fixation and permeabilization of cell membrane, rendering the cell unusable in a clinical environment.[4]

Recently, Raman microspectroscopy (rms) has been proposed for label-free noninvasive characterization of stem cells and their progeny.[8−14] Raman microspectroscopy combines the chemical specificity of Raman spectroscopy with the high spatial resolution of optical microscopy to provide detailed molecular information on cells without using labels or other invasive procedures.[15] Since water has a low Raman scattering cross section compared to most biomolecules,

Received: November 10, 2011
Accepted: March 13, 2012
Published: March 13, 2012

   dx.doi.org/10.1021/ac202994e | *Anal. Chem.* 2012, 84, 3155−3162

Raman spectra of cells have only a minimal background signal from water. Therefore, repeated measurements by Raman spectroscopy on viable cells maintained under physiological conditions are usually easier to carry out[16] compared to infrared absorption spectroscopy, where the strong absorption bands of water can distort the IR spectra.[17,18]

The basic hypothesis for using rms to discriminate between undifferentiated and differentiated cells relies on the expression of specific biomolecules by the cells at various stages of differentiation. Earlier studies reported that undifferentiated murine embryonic stem cells (mESCs) had higher concentration of mRNA compared to mESCs after 14 and 21 days of differentiation induced by removal of leukemia inhibitory factor.[8] These biochemical differences were related with the increased translation of dormant mRNAs during differentiation of the mESCs, by similarity with maturation of oocytes. Spectral differences related to nucleic acids were also reported for human ESCs (hESCs), but spectral differences were mostly associated to the smaller cytoplasm to nucleus ratio of undifferentiated cells compared to differentiated cells.[11] Comparison between different age groups of rhesus monkey mesenchymal cells derived from bone marrow also indicated a higher DNA and lower protein contribution in the Raman spectra of fetal compared to juvenile cells.[19] Spectral variations assigned to glycogen have also been reported for hESCs maintained under normal growth conditions in vitro.[12,20]

In addition to undifferentiated stem cells, rms has also been used for noninvasive phenotypic identification of individual cells or characterization of differentiated cell cultures derived from stem cells. Comparison between Raman spectra of human bone marrow stromal cells grown in purposed-built bioreactors over 21 days in basic and osteogenic culture media showed biochemical differences related to cell differentiation and mineralization.[21] Differences between the bone nodules formed by osteoblasts derived from mESCs and native tissues were also identified by Raman spectroscopy.[22] More recently, rms has also been proposed for phenotypic identification of individual cardiomyocytes within highly heterogeneous cell populations as commonly obtained during in vitro differentiation of hESCs. High accuracy discrimination models based on Raman bands associated mainly to glycogen and myofibrils allowed identification of hESC-derived cardimyocytes with sensitivity >96% and specificity >97%.[13] Although currently the measurement speed is limited to only few cells per second, these initial studies are starting to progress the Raman spectroscopy technique toward the development of Raman-activated cell sorting for label-free enrichment and purification of cell populations with well-defined phenotypes.[23]

In this study we have investigated the ability of rms to provide label-free spectral markers for noninvasive monitoring of the differentiation status of live NSCs in vitro, as well as detect spectral changes during their differentiation toward the glial phenotype. First, multivariate statistical models were developed to discriminate between undifferentiated NSCs and glial cells, then high spatial resolution Raman spectral imaging was used to correlate the observed spectral differences with molecular properties of NSCs.

MATERIALS AND METHODS

Cell Culture. Cell culture reagents were purchased from Invitrogen (Paisley, UK) unless otherwise stated. Mouse neural stem cells were cultured as described elsewhere.[4] Briefly, cells were maintained in NSC medium prepared with DMEM/F12 and Neurobasal medium (1:1), N2, B27, Pen/Strep, bFGF (20 ng/mL) and EGF (20 ng/mL, Sigma, UK). To passage the cultures, the cells were treated with 1 mL of Accutase (Patricell Ltd., Nottingham, UK) and the sample was incubated at 37 °C for 5 min. After a PBS wash, the pellet was resuspended in fresh medium and transferred to a new vessel. Culture stocks were routinely split 1 in 3. For Raman analysis, cells were seeded on the MgF_2 coverslips of the cell-chambers after coating with Matrigel (Becton Dickinson) to promote cell adhesion. For in vitro differentiation, NSC medium was replaced with medium containing DMEM/F12 and Neurobasal (1:1), 1% FCS, Pen/Strep. Fresh medium was added every 2 days, taking care not to disturb the monolayer. For high resolution Raman measurements, cells were fixed with 4% ice-cold paraformaldehyde and stored at 4 °C until analysis.

Immunostaining. Samples were washed in PBT (phosphate buffer saline PBS + 0.1% Tween-20 (Sigma)), blocked for 1 h in 1% blocking solution (PBT+0.1% FCS), and incubated overnight at 4 °C with an anti-GFAP antibody (Dako, Ely, UK) diluted 1/100 in 1% blocking solution. After extensive washing in PBT for 40 min, samples were incubated with a fluorescein-conjugated secondary antibody (Vector Laboratories, Peterborough, UK) for 1 h, washed for 1 h in PBS, and kept in PBS containing 1 μg/mL Hoechst 33342 (Sigma) until imaging. For the viability tests, a dead/live fluorescence imaging kit was used (Invitrogen, UK). On the basis of this test, the green SYTO10 dye stained the nuclei of viable cells while the red membrane-impermeable dye (ethidium homodimer-2) stained the nucleic acids for the cells with compromised plasma membrane.

Raman Microspectroscopy Measurements. For Raman measurements of live cells under physiological conditions (culture medium, 37 °C temperature, 5% CO_2), a Raman microspectrometer equipped with an environmental enclosure (Solent, Segensworth, UK) was used. The instrument was based on an inverted microscope (IX 71, Olympus, Essex, UK) with a 60×/NA 0.90 water-immersion objective (Olympus), a 785 nm ~170 mW diode laser (at sample) (Toptica Photonics, Munich, Germany), a spectrometer equipped with a 830 lines/mm grating and cooled deep-depletion back-illuminated CCD detector (Andor Technologies, Belfast, UK) and an automated step-motor stage (Prior, Cambridge, UK). For the high spatial resolution spectral images, a second confocal Raman microspectrometer was used consisting of an inverted optical microscope (Ti-Eclipse, Nikon, UK) equipped with a water-immersion objective (60×/NA 1.2) (Olympus, Essex, UK), a 710 nm Gaussian-beam Ti:sapphire laser (Spectra-Physics) with ~170 mW at sample, a high-precision piezo-electric XY stage (PI, Germany). The optical microscope was connected by means of a 50 μm diameter optical fiber to the same spectrometer. The laser beam was expanded to fill the back-aperture of the objective and to enable focusing the laser beam to a diffraction limited spot on the sample.

Both instruments were calibrated prior to each experiment using a standard tylenol sample, and the spectral resolution in the 600−1800 cm^{-1} region was ~1.5 cm^{-1}. Purpose designed titanium cell-chambers were built (25 mm diameter and 15 mm height), which incorporated a MgF_2 coverslip (0.17 mm thick) at the bottom to enable acquisition of Raman spectra of the cells using the inverted optical configuration. For the live cells, the Raman spectrum of each individual cell represented the average of a total of 625 spectra obtained by raster-scanning the cell through the laser focus in 2 μm steps (equivalent to a grid

of 25 by 25 points). The acquisition time at each position was 1 s. After the acquisition of Raman spectra was completed, the position coordinates of each cell were recorded, the cells were fixed and prepared for immunostaining (phenotypic marker and cell nucleus). The phenotype of the cells was established using a wide-field fluorescence staining system integrated on the Raman microscope. Since the staining with the fluorescence dyes required the removal of the cells from the Raman microscope, the repositioning of the cells was based on two marks engraved at the edges of the cell chamber and the recorded coordinates of the cells. The accuracy in repositioning the cells by this procedure was ~5 μm. For imaging fixed cells, raster scans were carried out at step sizes of 0.5 and 1 μm with integration time of 3 s/pixel.

Nucleic acids were purchased from Sigma Aldrich (UK) and used without further purification: Baker's yeast RNA (cat no. 83853) and calf thymus DNA (cat no. D4522). Raman spectra were measured as solutions in water (resistivity 18.2 MΩcm) at concentrations 10 mg/mL for RNA and 30 mg/mL for DNA at 170 mW laser power and 3 s integration time. A similar cell chamber was used for these measurements as for the measurements on the cells. The calibration curve for RNA was built by using three measurements at each concentration value using a laser power of 170 mW and acquisition time of 30 s to increase the signal-to-noise ratio. Since the acquisition times for the Raman spectra of cells were 3 s/pixel, the intensity of the Raman spectra of RNA used for the calibration was divided by a factor of 10 to allow direct comparison.

Data Analysis and Processing. Data preprocessing consisted of removal of spectra containing cosmic rays, background subtraction, and normalization. The average of the Raman spectra measured at points outside of the cell (automatically identified using a *k*-means clustering analysis) represented the background spectrum (contributions from the culture medium, MgF_2 coverslip and microscope objective). The Raman spectrum representative of each cell was obtained by algebraic subtraction of the background spectrum from the average of the Raman spectra at all positions inside the cell. All Raman spectra were then normalized using the standard normal variance method.[13,31]

The Raman spectra of cells were analyzed by principal component analysis (PCA) and linear discriminant analysis (LDA). Spectral images corresponding to selected Raman bands were obtained by calculating the area under the spectral bands after the subtraction of the background spectrum and estimated local linear baselines and representing the integrated intensity value spectral region at each measurement position in the cell. The following spectral regions were used: 766−796 cm^{-1} for the 788 cm^{-1} band, 798−821 cm^{-1} for the 813 cm^{-1} band, and 1411−1510 cm^{-1} for the 1450 cm^{-1} band. Prior to calculation of band areas, the singular value decomposition method was used to reduce the noise in the Raman spectra[24] while still maintaining 80−90% of the original information.

RESULTS AND DISCUSSION

Discrimination between Undifferentiated Neuroprogenitor and Glial Cells. The first aim of the study was to identify Raman spectral bands which enable discrimination between undifferentiated NSCs and NSC-derived glial cells by using noninvasive Raman spectral measurements on live cells. Although previous studies using 785 nm lasers to measure Raman spectra of other cell types showed that no damage was induced to the cells,[13,25] viability tests on selected NSCs and NSC-derived glial cells were carried out after completion of the Raman measurements. The results of the fluorescence staining tests confirmed that the cells remained viable at the end of the Raman measurements (Supporting Information Figure S-1).

Figure 1 presents the average Raman spectra and immunofluorescence images of two typical live glial cells and two groups

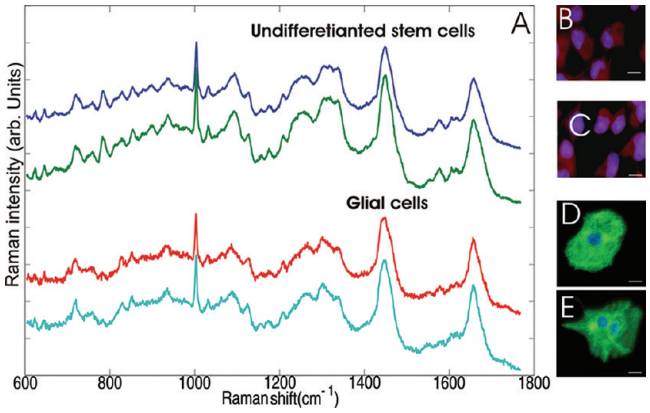

Figure 1. (A) Typical Raman spectra measured for undifferentiated neural stem cells and glial cells and the corresponding fluorescence staining of the cells confirming their phenotypes: (B and C) undifferentiated neural stem cells, blue = nuclei, red = nestin; (D and E) glial cells, blue = nuclei, green = GFAP.

of NSCs. When carrying out Raman spectral measurements on individual live NSCs, it was found that cell motility was significant over the measurement time (~10 min). Therefore, to reduce errors due to cell motility, the Raman spectra of NSCs were recorded as full raster scans over individual cells or groups of 5−6 cells in proximity, for which motility was observed to be considerably reduced. No differences were observed in the Raman spectra of individual NSCs or NSCs in groups (Supporting Information Figure S-2). Because the motility of the glial cells during the Raman measurements was not significant and because these cells are considerably larger than the NSCs, the glial cells were measured individually. After Raman measurements, all cells were fixed and stained to confirm the phenotype: nestin was used for undifferentiated NSCs and GFAP was used for glial cells. The phenotypic confirmation was carried out to ensure that no errors due to potential population heterogeneities were included in the Raman spectral model. The Raman spectra in Figure 1A show that the sampling method used in this study led to high signal-to-noise spectra which accounted for the molecular heterogeneity of the cells. Therefore, such average Raman spectra are representative of an entire cell or group of cells analyzed. The Raman spectra of both cell types consist of typical Raman bands of cellular biomolecules (nucleic acids, protein, lipids, and carbohydrates) and are consistent with previous reports on other cell types.[15] Spectral differences between the glial and NSC populations can be observed in particular in the 700−830 cm^{-1} region, which contains contributions mainly from nucleic acids. However, to confirm these spectral differences, Figure 2 presents the average Raman spectra of 120 NSCs (19 groups) and 27 differentiated glial cells along with the computed difference spectrum (average spectrum for all NSCs minus average spectrum of all glial cells). Several Raman bands corresponding to nucleic acids can be identified in the difference spectrum.

dx.doi.org/10.1021/ac202994e | *Anal. Chem.* 2012, 84, 3155−3162

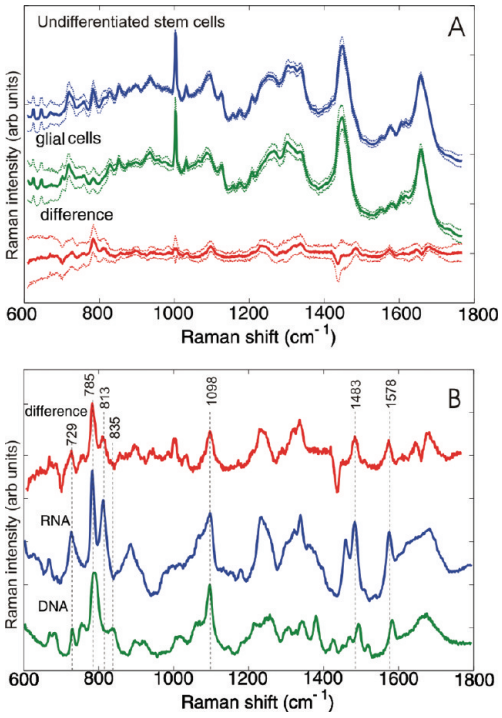

Figure 2. (A) Average Raman spectra of undifferentiated stem cells and glial cells and their computed difference. The side lines represent the standard deviation calculated at each wavenumber. (B) Comparison between the computed difference spectrum in A and the Raman spectra measured from purified RNA and DNA.

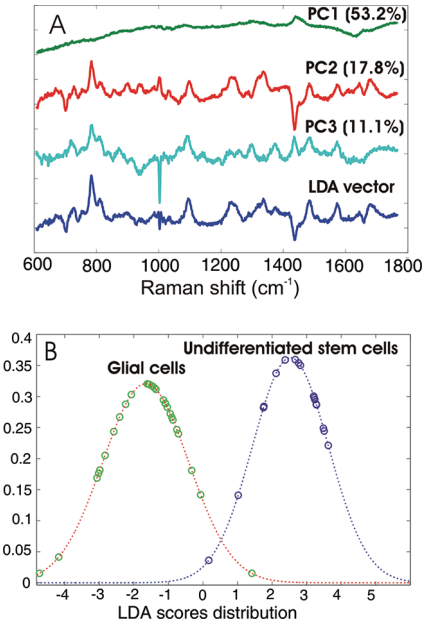

Figure 3. (A) Loadings of the first three PCA components (PC1, PC2, and PC3) used for building the LDA discrimination vector to maximize the discrimination between the Raman spectra of the undifferentiated NSCs and glial cells. The variance captured by each principal component is shown in the brackets. (B) Distribution of LDA scores for undifferentiated stem cells (purple dots) and glial cells (green dots).

A comparison between the difference spectrum and the Raman spectra of DNA and RNA in water is presented in Figure 2B. Based on previous reports using X-diffraction measurements on nucleic acids solution at neutral pH and equilibrium conditions (as used in our experiments), the DNA adopts a B-conformation while the RNA adopts a A-conformation.[26,27] Raman bands associated to the DNA and RNA bases can be identified at 729 (adenine), 782 and 785 (uracil, cytosine), and 1578 cm^{-1} (guanine and adenine).[28] Raman bands corresponding to the nucleic acid backbone can also be identified and used for identification of the conformation of the nucleic acids. B-conformation DNA elicits a strong band at 788 cm^{-1} and a shoulder at 835 cm^{-1} corresponding to the symmetric and asymmetric O−P−O phosphodiester stretching vibrations. For A-DNA and RNA, the symmetric vibration shifts to 813 cm^{-1} and the band corresponding to the asymmetric stretching vanishes.[29,30] In addition, a Raman band at 1098 cm^{-1} can also be identified corresponding to the PO_2^- vibrations. These results suggest that the main spectral differences between NSCs and differentiated glial cells rely on a higher concentration of nucleic acids in NSCs.

A multivariate spectral model based on the principal component analysis (PCA) followed by linear discriminant analysis (LDA) was developed to enable spectral discrimination between the two cell types. The loading spectra corresponding to the first three principal components capturing 82.1% of spectral variation are shown in Figure 3. For the LDA model, only PC1, PC2, and PC3 were used as other PCs either consisted only of broad bands characteristic to the culture medium or were dominated by noise; therefore, they did not improve the discrimination between the two cell types. While the loading of PC1 captured significant variance in the baseline among all cells, PC2 and PC3 consisted mainly of features which can be related to cellular components which can also be identified in the computed difference spectrum between NSCs and glial cells. The linear discriminant analysis loading which maximized the discrimination between the NSCs and glial cells (Figure 3A) is dominated by features corresponding to the nucleic acids. The probability distribution for the LDA scores (Figure 3B) shows a clear distinction between NSCs and glial cells.

To determine the accuracy for phenotypic identification of NSCs, cross-validation (CV) was used to determine the sensitivity and specificity parameters for a certain target sensitivity or specificity. The leave-one-out CV showed that the LDA spectral model can discriminate between NSCs and glial cells with 89.4% sensitivity and 96.4% specificity.

Assignment and Quantification of the Raman Spectral Markers. The computed difference spectrum in Figure 2 indicates that significant molecular changes related to nucleic acids can be identified between undifferentiated NSCs and glial cells. In particular, one can highlight the Raman band at 813 cm^{-1} which has been assigned to the symmetric stretching of the phosphodiester bonds in nucleic acids with A-conformation. However, this spectral difference could be related either to conformational changes of DNA from B-form to A-form or due to changes related to the RNA concentration.

A decrease in the 813 cm^{-1} band was also detected by rms in the case of spontaneous differentiation of mESCs over a 21 day period.[8] The intense 813 cm^{-1} band in undifferentiated mESCs was suggested to be related to repressed translation of mRNAs in the embryonic stem cells followed by increased mRNA translation during the differentiation. Spectral differences associated to nucleic acids were also found in undifferentiated

dx.doi.org/10.1021/ac202994e | Anal. Chem. 2012, 84, 3155−3162

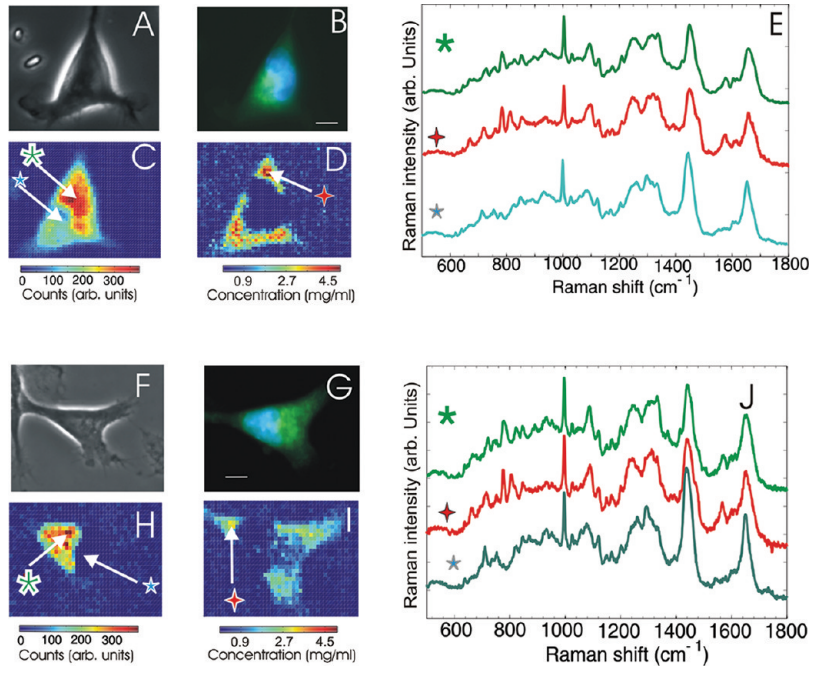

Figure 4. Phase contrast images (A and F), nuclei(blue)/nestin(green) fluorescence staining (B and G) and Raman spectral images corresponding to the 788 cm^{-1} band (C and H) and 813 cm^{-1} band (D and I) for two typical fixed undifferentiated neural stem cells. The Raman images in D and I were calibrated using the curve in Figure 6. (E and J) Individual Raman spectra taken from selected positions of the nuclei (green star), cytoplasm regions rich in RNA (red star), and cytoplasm regions rich in phospholipids (blue star) (scale bars: 10 μm).

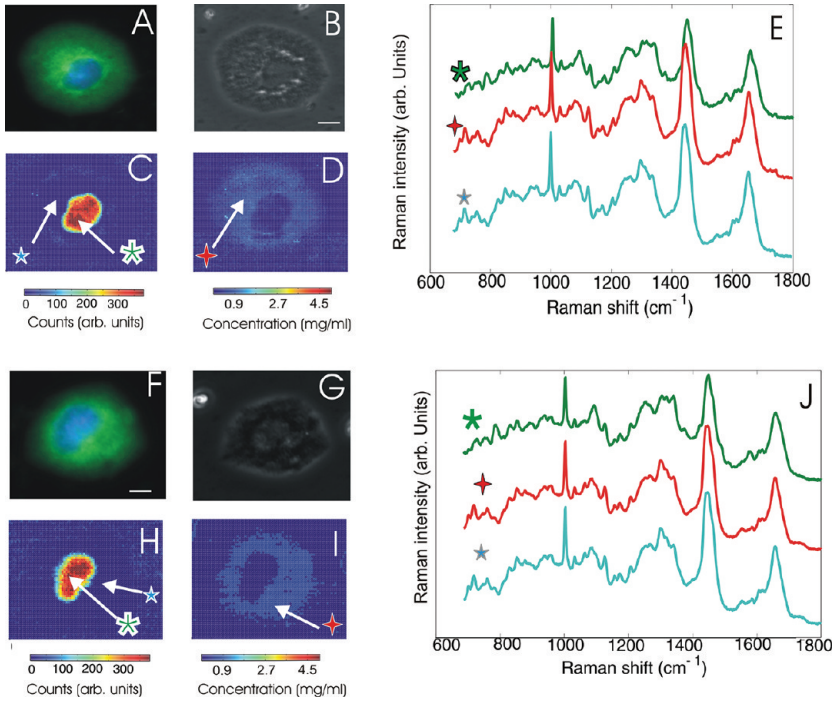

Figure 5. Phase contrast images (A and F), DAPI(blue)/GFAP(green) fluorescence staining (B and G), and Raman spectral images corresponding to the 788 cm^{-1} band (C and H) and 813 cm^{-1} band (D and I) for two typical fixed glial cells. The Raman images in D and I were calibrated using the curve in Figure 6. (E and J) Individual Raman spectra taken from selected positions of the nuclei (green star) and two positions in the cytoplasms (red and blue star) (scale bars: 10 μm).

and differentiated hESC and mesenchymal stem cells[11,19] and were attributed to a higher nucleus to cytoplasm ratio in the undifferentiated cells and associated to the increased proliferation rates compared to differentiated cells. However, these studies recorded only single point measurements for individual cells and did not include spatially resolved Raman spectra needed to determine whether the increased signals corresponding to nucleic acids was associated to the cell nuclei (mainly DNA) or cytoplasm (RNA), or alternative methods to distinguish between RNA and A-form DNA.

One of the important features of confocal rms is that it allows the mapping of the biomolecules within individual cells with

dx.doi.org/10.1021/ac202994e | *Anal. Chem.* 2012, 84, 3155–3162

diffraction limited spatial resolution. Comparison between Raman spectral images corresponding to specific biomolecules and fluorescence staining also allows a better correlation between Raman spectral information and cellular components.[13,31] In this case, such comparison was carried out to establish whether the spectral differences were related to DNA conformational changes (most DNA is located in the nucleus) or to RNA concentration (cytoplasmic RNA). Raman spectral maps for 788 and 813 cm^{-1} were measured and compared with fluorescence staining for the nucleus and cytoplasm for the same cells. However, Raman imaging requires raster scanning the cell through the laser focus and collection of a full spectrum at each position. Although individual Raman spectra with sufficient signal-to-noise ratio can be acquired using integration times as short as 500 ms/pixel (Supporting Information Figure S-3), a Raman mapping using step sizes of half the diffraction limit (500 nm) requires 20 min. To avoid cell movement during the Raman imaging and thus enable accurate comparison between the Raman maps and fluorescence images, the measurements were carried out on fixed NSCs and glial cells. The comparison between the Raman spectra of fixed and live cells shows that paraformaldehyde fixation of cells did not significantly affect the Raman spectra (Supporting Information Figure S-4), findings which agree with published reports on other cell types.[32,33]

Figure 4 presents the spectral maps of two typical NSCs corresponding to the 788 and 813 cm^{-1} Raman bands along with the corresponding phase contrast and fluorescence staining of the cell nuclei (DAPI) and cytoplasm (nestin). Compared to the DAPI staining, the cell region of high 788 cm^{-1} intensity is larger than the cell nuclei because this band consists of an overlap between the C and U ring vibration at 785 cm^{-1} and the O−P−O symmetric stretch in B-DNA. Therefore, the Raman images corresponding to the 788 cm^{-1} highlight regions rich in both DNA and RNA. However, comparison between the fluorescence images and the Raman images corresponding to the 813 cm^{-1} Raman band shows that the cell regions where these bands have high intensity correspond to the cytoplasms. To confirm the presence of the 813 cm^{-1} band in the cytoplasm of the NSCs, individual Raman spectra from locations of intense 788 and 813 cm^{-1} Raman bands are also presented and compared to spectra at other positions in the cytoplasm with reduced nucleic acid contributions (spectra dominated by other biomolecules such as proteins and lipids).

On the basis of these results, it can be concluded that the assignment of the 813 cm^{-1} band corresponds to cytoplasm RNAs and not to conformational changes of the DNA. A confirmation of these findings for live NSCs is presented in Supporting Information Figure S-5. However, to reduce the errors due to cell motility when comparing Raman and fluorescence images, the Raman spectral images were recorded at a lower spatial resolution (2 μm step size, total imaging time ~6 min).

Figure 5 presents similar comparisons between Raman spectral maps of nucleic acids and fluorescence staining for two typical differentiated glial cells derived from NSCs. In this case, a very close similarity can be observed between the Raman maps corresponding to the 788 cm^{-1} band and the DAPI images of the nuclei. These results indicate that, contrary to NSCs, contribution from nucleic acids in the glial cells can only be detected in the nucleus. Therefore, the concentration of the RNA in the cytoplasm of glial cells is considerably lower than in NSCs, becoming below the detection limit of our instrument (unity signal-to-noise ratio).

The origin of these spectral differences which allow the assessment of the differentiation status of NSCs by rms may be attributed to two main properties of NSCs when compared to differentiated cells: lower cytoplasm volume and overall higher amount of cytoplasmic RNA. Although an accurate evaluation of cytoplasm volume is difficult, we attempted an estimation of the ratio between the cytoplasm volumes between NSCs and glial cells based on the fluorescence images and selected Raman maps. Assuming that the intensity of the 1450 cm^{-1} band corresponding to CH_2 vibrations in all biomolecules can be used as a measure of biomass, comparison between the Raman maps for this band indicated no significant differences between the heights of NSCs and glial cells (Figure 6A–D). However,

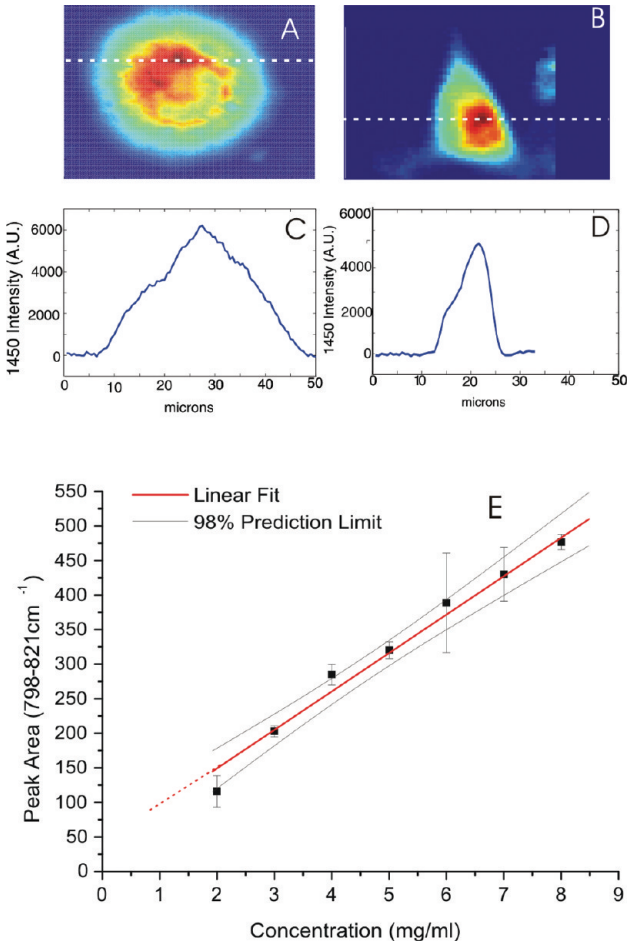

Figure 6. Raman spectra maps corresponding to the 1450 cm^{-1} band for a glial cell (A), undifferentiated neural stem cell (B), and their corresponding profiles at the positions indicated by the white dotted lines (C and D). (E) Calibration curve for the 813 cm^{-1} Raman band using purified RNA solutions in water.

based on the fluorescence images, it can be estimated that on average, the cytoplasm of the NSCs is approximately 4.5 times smaller than the cytoplasm of the glial cells. On the basis of these estimates, the increase in cytoplasmic volume for the glial cells would lead to a maximum ~4.5 fold decrease in the concentration of cytoplasmic RNA if the overall amount of RNA would remain unchanged during the differentiation. Figure 6E presents a calibration curve for the 813 cm^{-1} Raman

dx.doi.org/10.1021/ac202994e | Anal. Chem. 2012, 84, 3155−3162

band corresponding to RNA solutions in water as a function of concentration.

According to this calibration curve, the maximum concentration of RNA in the cytoplasm of NSCs ranges from 3 to 5 mg/mL (accuracy in this range is ±0.4 mg/mL) while for glial cells the concentration becomes lower than the detection limit of RNA for our instrument, which is ∼1 mg/mL. This finding was somehow surprising considering that the rRNA represents the dominant type of RNA in cells and most somatic cells have abundant ribosomes. However, the estimates of the cell volumes indicate that the increase in the cytoplasm volume by a factor of 4.5 may account for a decrease in the cytoplasm RNA concentration during the differentiation of NSCs to the glial phenotype.

The higher intensities of Raman bands corresponding to RNA in NSCs may also be related to a higher amount of RNA in the cytoplasm of undifferentiated cells compared to fully differentiated cells. Early studies on lineage progenitors have reported a change in RNA content during the differentiation process. Histological analysis of embryonic brain explants has shown that neuroepithelial progenitor populations in the ependymal layer have a higher total RNA content than their mature differentiated progeny.[34] Increased concentration of nontranslated mRNAs corresponding to the post-transcriptional control of genes has been related to neurogenesis[35] and neuronal function,[36] as well as stem cell proliferation and embryogenesis.[37,38] For example, high abundance of proteins which repress the translation of mRNAs and maintained the undifferentiated state of NSCs have been found in the cytoplasms of these cells.[35] In a different model, epidermal progenitors have similarly been reported to display higher RNA amounts than terminally differentiated keratinocytes.[39] Interestingly, the fine dynamics of these variations over the differentiation process appears to involve a transient increase before a significant drop in RNA amounts observed in mature differentiated lineages.

More recently, the importance of RNA subtypes including long noncoding RNAs and microRNAs has been highlighted in the context of cell differentiation.[40−43] Data gathered from mouse ES cells, and more recently NSCs, suggest that such noncoding regulatory RNAs are dynamically regulated during the differentiation process. Further real time analysis of Raman spectral patterns in time-course differentiation experiments will allow us to finely monitor and quantify subtle changes in nucleic acids in a noninvasive manner, and monitor the cell status within the differentiation continuum.

CONCLUSION

rms is an attractive technique for noninvasive characterization of individual live cells in vitro. In this study, rms was used to identify label-free spectral markers for noninvasive monitoring the differentiation status of live neural stem cells (NSCs) in vitro. Such techniques are urgently needed for the characterization of cell populations and assessing their differentiation status noninvasively. Principal component analysis (PCA) and linear discriminant analysis (LDA) models based on Raman spectra of undifferentiated NSCs and NSC-derived glial cells enabled discrimination of NSCs with 89.4% sensitivity and 96.4% specificity. The differences between Raman spectra of NSCs and glial cells indicated that the discrimination between these cell types is based on higher concentration of nucleic acids in NSCs compared to glial cells. Comparison between Raman mapping of DNA and RNA showed that the regions with largest spectral differences are located in the cytoplasm of the NSCs and therefore can be assigned to cytoplasmic RNAs. These results are in agreement with previous studies on mouse embryonic stem cells which indicated a significant decrease in RNA during differentiation in vitro. Spectral calibrations built using RNA solutions in water allowed quantification of RNA concentration in the cytoplasm of the cells. It was found that the concentrations as high as 4 mg/mL were found in the cytoplasm of NSCs while the corresponding values for glial cells were below the detection limit of our instrumentation (∼1 mg/mL).

On the basis of previous literature reports, we propose that the observed high concentration of RNAs in NSCs is related to the repressed translation of mRNAs and higher concentration of large noncoding RNAs in the cytoplasm of undifferentiated stem cells as well as the increase in cytoplasm volume during differentiation. While this study demonstrates the potential of rms for label-free assessment of live NSCs in vitro, further studies are required to establish the exact origin of the increased contribution of the cytoplasmic RNA in the undifferentiated population.

ASSOCIATED CONTENT

Supporting Information

Supporting information includes the following: (Figure S-1) Viability tests of NSCs and glial cells after rms. (Figure S-2) Comparison between Raman spectra of live NSCs measured as individual cells and group of cells. (Figure S-3) Demonstration of Raman imaging of cytoplasmic RNA in undifferentiated neural stem cells at 500 ms/pixel integration time. (Figure S-4) Comparison between Raman spectra of live cells and cells fixed with paraformaldehyde. (Figure S-5) Evidence of cytoplasm regions of high RNA concentrations in live undifferentiated neural stem cells. This material is available free of charge via the Internet at http://pubs.acs.org.

AUTHOR INFORMATION

Corresponding Author

*E-mail: ioan.notingher@nottingham.ac.uk (I.N.) or virginie.sottile@nottingham.ac.uk (V.S.).

Notes

The authors declare no competing financial interest.

ACKNOWLEDGMENTS

This study was funded by grant awards from the University of Nottingham and the Biotechnology and Biological Sciences Research Council UK (BB/G010285/1). V.S. is indebted to the Anne McLaren fellowship scheme (University of Nottingham) and to the Alzheimer's Society for their support, past and present.

REFERENCES

(1) Kalladka, D.; Muir, K. W. *Neurochem. Int.* **2011**, *59* (3), 367−370.
(2) Lilienfeld, D. E.; Perl, D. P. *Neuroepidemiology* **1994**, *13* (4), 179−86.
(3) Rossi, F.; Cattaneo, E. *Nat. Rev. Neurosci.* **2002**, *3* (5), 401−9.
(4) Alcock, J.; Sottile, V. *Cell Res.* **2009**, *19*, 1324−1333.
(5) Arocena, M.; Zhao, M.; Collinson, J. M.; Song. *B. J. Neurosci. Res.* **2010**, *88*, 3267−3274.
(6) Fox, J. L. *Nat. Biotechnol.* **2008**, *26*, 598−599.
(7) Fukuda, H.; Takahashi, J.; Watanabe, K.; Hayashi, H.; Morizane, A.; Koyanagi, M.; Sasai, Y.; Hashimoto, N. *Stem Cells* **2006**, *24* (3), 763−771.

(8) Notingher, I.; Bisson, I.; Bishop, A. E.; Randle, W. L.; Polak, J. M.; Hench, L. L. *Anal. Chem.* **2004**, *76* (11), 3185−3193.
(9) Zuser, E.; Chernenko, T.; Newmark, J.; Miljković, M.; Diem, M. *Analyst* **2010**, *135* (12), 3030−3033.
(10) Chan, J. W.; Deborah, K. Lieu; Huser, T.; Li, A. L. *Anal. Chem.* **2009**, *81* (4), 1324−1331.
(11) Schulze, H. G.; Konorov, S. O.; Caron, N. J.; Piret, J. M.; Blades, M. W.; Turner, R. F. B. *Anal. Chem.* **2010**, *82* (12), 5020−7.
(12) Konorov, S. O.; Schulze, G.; Piret, J. M.; Turner, R. F. B; Blades, M. W. *J. Raman Spectrosc.* **2011**, *42* (5), 1135−1141.
(13) Pascut, F. C.; Huey, T. G.; Welch, N.; Buttery, L. D.; Denning, C.; Notingher, I. *Biophys. J.* **2011**, *100* (1), 251−9.
(14) Konorov, S. O.; Schulze, H. G.; Caron, N. J.; Piret, J. M.; Blades, M. W.; Turner, R. F. B. *J. Raman Spectrosc.* **2010**, *42* (4), 576−579.
(15) Notingher, I.; Hench, L. L. *Exp. Rev. Med. Dev.* **2006**, *3* (2), 215−234.
(16) Zoladek, A.; Pascut, F. C.; Patel, P.; Notingher, I. *J. Raman Spectrosc.* **2011**, *42* (3), 251−258.
(17) Kuimova, M. K.; Chan, K. L.; Kazarian, S. G. *Appl. Spectrosc.* **2009**, *63* (2), 164−171.
(18) Marcsisin, E. J.; Uttero, C. M.; Miljković, M.; Diem, M. *Analyst* **2010**, *135*, 3227−3232.
(19) Kim, B. S.; Lee, C. C.; Christensen, J. E.; Huser, T. R.; Chan, J. W.; Tarantal, A. F. *Stem Cells Dev.* **2008**, *17* (1), 185−198.
(20) Konorov, S. O.; Schulze, H. G.; Atkins, C. G.; Piret, J. M.; Aparicio, S. A.; Turner, R. F. B.; Blades, M. W. *Anal. Chem.* **2011**, *83* (16), 6254−8.
(21) Pully, V. V.; Lenferink, A.; van Manen, H. J.; Subramaniam, V.; van Blitterswijk, C. A.; Otto, C. *Anal. Chem.* **2010**, *82* (5), 1844−50.
(22) Gentleman, E.; Swain, R. J.; Evans, N. D.; Boonrungsiman, S.; Jell, G.; Ball, M. D.; Shean, T. A. V.; Oyen, M. L.; Porter, A.; Stevens, M. M. *Nat. Mater.* **2009**, *8* (9), 763−70.
(23) Pascut, F. C.; Goh, H. T.; George, V.; Denning, C.; Notingher, I. *J. Biomed. Opt.* **2011**, *16*, 045002.
(24) Uzunbajakava, N.; Lenferink, A.; Kraan, Y.; Volokhina, E.; Vrensen, G.; Greve, J.; Otto, C. *Biophys. J.* **2003**, *84* (6), 3968−3981.
(25) Zoladek, A. B.; Johal, R. K.; Garcia-Nieto, S.; Pascut, F. C.; Ghaemmaghami, A.; Notingher, I. *Analyst* **2010**, *135*, 3205−3212.
(26) Davies, D. D. *Annu. Rev. Biochem.* **1967**, *36*, 321−364.
(27) Arnott, S. *Prog. Biophys. Mol. Biol.* **1970**, *21*, 265−319.
(28) Tu, A. T. *Raman Spectroscopy in Biology: Principles and Application*; Wiley: New York, 1982.
(29) Erfurth, S. C.; Kiser, E. J.; Peticolas, W. L. *Proc. Natl. Acad. Sci. U.S.A.* **1972**, *69* (4), 938−941.
(30) Benevides, J. M.; Thomas, G. J. Jr. *Nucleic Acids Res.* **1983**, *11* (16), 5747−61.
(31) Matthäus, C.; Chernenko, T; Newmark, J. A.; Warner, C. M.; Diem, M. *Biophys. J.* **2007**, *93*, 668−673.
(32) Chan, J. W.; Taylor, D. S.; Thompson, D. L. *Biopolymers* **2009**, *91* (2), 132−9.
(33) Mazur, A. I.; Marcsisin, E. J.; Bird, B.; Miljković, M.; Diem, M. *Anal. Chem.* **2012**, *84* (3), 1259−1266.
(34) Birge, W. J. *Anat. Rec.* **1962**, *143*, 147−55.
(35) Okano, H.; Kawahara, H.; Toriya, M.; Nakao, K.; Shibata, S.; Imai, T. *Exp. Cell Res.* **2005**, *306*, 349−356.
(36) Finkenstadt, P. M.; Kang, W. S.; Jeon, M.; Taira, E.; Tang, W.; Baraban, J. M. *J. Neurochem.* **2000**, *75*, 1754−1762.
(37) Kuersten, S.; Goodwin, E. B. *Nat. Rev. Genet.* **2003**, *4*, 626−637.
(38) Macnicol, M. C.; Macnocol, A. M. *Mol. Reprod. Dev.* **2010**, *77*, 662−669.
(39) Staiano-Coico, L.; Higgins, P. J.; Darzynkiewicz, Z.; Kimmel, M.; Gottlieb, A. B.; Pagan-Charry, I.; Madden, M. R.; Finkelstein, J. L.; Hefton, J. M. *J. Clin. Invest.* **1986**, *77* (2), 396−404.
(40) Dinger, M. E.; Amaral, P. P.; Mercer, T. R.; Pang, K. C.; Bruce, S. J.; Gardiner, B. B.; Askarian-Amiri, M. E.; Ru, K.; Soldà, G.; Simons, C.; Sunkin, S. M.; Crowe, M. L.; Grimmond, S. M.; Perkins, A. C.; Mattick, J. S. *Genome Res.* **2008**, *18* (9), 1433−45.
(41) Mercer, T. R.; Qureshi, I. A.; Gokhan, S.; Dinger, M. E.; Li, G.; Mattick, J. S.; Mehler, M. F. *BMC Neurosci.* **2010**, *5*, 11−14.
(42) Pauli, A; Rinn, J. L.; Schier, A. F. *Nat. Rev. Genet.* **2011**, *12* (2), 136−49.
(43) Guttman, M.; Donaghey, J.; Carey, B. W.; Garber, M.; Grenier, J. K.; Munson, G.; Young, G.; Bergstrom, L. A.; Ach, R.; Bruhn, L.; Yang, X.; Amit, I.; Meissner, A.; Regev, A.; Rinn, J. L.; Root, D. E.; Lander, E. S. *Nature* **2011**, *477*, 295−300.